PAN ARCHIVES OF ACOUSTICS
Vol. **39**, No. 4, pp. 453–465 (2014)

DOI: 10.2478/aoa-2014-0049

Acoustical Boundary Elements: Theory and Virtual Experiments

Rafael PISCOYA, Martin OCHMANN

University of Applied Sciences
13353 Berlin, Germany; e-mail: piscoya@beuth-hochschule.de

(*received October 7, 2014; accepted December 17, 2014*)

This paper presents an overview of basic concepts, features and difficulties of the boundary element method (BEM) and examples of its application to exterior and interior problems. The basic concepts of the BEM are explained firstly, and different methods for treating the non-uniqueness problem are described. The application of the BEM to half-space problems is feasible by considering a Green's Function that satisfies the boundary condition on the infinite plane. As a special interior problem, the sound field in an ultrasonic homogenizer is computed. A combination of the BEM and the finite element method (FEM) for treating the problem of acoustic-structure interaction is also described. Finally, variants of the BEM are presented, which can be applied to problems arising in flow acoustics.

Keywords: Boundary elements, Green's function, non-uniqueness.

1. Introduction

The Boundary Element Method (BEM) is a well-established numerical technique with successful application to the calculation of the sound radiation from vibrating bodies and to the scattering of sound waves. By means of the BEM, it is possible to perform "virtual experiments" in order to study the effect of parameter variations. Such studies may lead to saving of expenses since only the optimized configurations need to be constructed and measured. In this work, we do not intend to make a review of the development of the BEM in acoustics but to demonstrate its features and capabilities by showing the results of such virtual experiments performed in our recent research projects. A comparison of the BEM with other deterministic methods like the FEM is not a purpose of the paper either. A comparison in that regard can be found for example in Bolejko and Dobrucki (2006).

In this work, we treat only the direct BEM approach where the unknowns are the sound pressure and particle velocity. The indirect approach, where the unknowns are the jumps of the acoustical variables instead of the variables themselves, can be found for example in the book of Wu (2000). The indirect BEM is used mostly when very thin objects are part of the structure. An example of application of the indirect approach can be found in Dobrucki and Plaskota (2007).

The most important feature of the BEM lies in the fact, that only the surface of radiating or scattering bodies need to be discretized. On one hand, the surface discretization makes the method very suitable for treating exterior problems. On the other hand, specifically for the exterior problems, the BEM present problems with the non-uniqueness of the solutions at certain critical frequencies, which are of pure numerical nature but can be overcome using regularization techniques. We show those techniques and present two examples of the application of the BEM for exterior problems, one for the free-space and other for the half-space. The first example is an academic one, i.e. the radiation of a dipole source and the second example is a more applied one, which is the computation of the horn effect in tyre noise determination. Other and diverse examples of the applications of the BEM can be found in the literature, for example the calculation of sound radiation of an engine transmission cover (Tinnsten et al., 2001), the prediction of noise of power transformers (Rausch *et al.*, 2002), the study of sound distribution in urban areas (Baulac *et al.*, 2006) or the estimation of the transmission loss of a sound barrier (Monazzam *et al.*, 2010), to mention only a few.

The BEM is also well applicable to interior problems. Since the number of surface elements increases with frequency, the maximum frequency that can be considered depends on the storage capacity of the computer. In this regard, the surface discretization allows

in some cases to attain a higher frequency range than a volume discretization, especially if a tailored Green's function is available. As a numerical experiment, we compute the sound field in an ultrasonic homogenizer where our parameter to be studied is the boundary condition at the glass walls. Other examples of the use of the BEM in interior problems can be found in Suzuki *et al.* (1989), Utsuno *et al.* (1990) or Tadeu *et al.* (2012).

The BEM can be combined with other methods in order to develop hybrid methods in which the BEM computes the propagation of sound waves due to sound sources or vibrating surfaces obtained by other methods. A very common combination is the FEM-BEM applied to problems of acoustic-structure interaction. We present such combination applied to the calculation of the airborne transmission loss of thin plates in a duct and in a test facility. Other typical example of that combination is the scattering of submerged objects (e.g. Seybert, 1990). Additionally we present here also a hybrid method that combines the Large Eddy Simulation (LES) with the BEM to compute combustion noise. Problems involving flows, especially non-uniform ones, have become very important in actual engineering applications but are very difficult to solve. That type of problems has lead to the emergence of the Computational Aeroacoustics (CAA), a discipline that looks to calculate the sound due to turbulent flows using numerical methods, mainly by applying hybrid approaches. Two other examples of works using the BEM in aeroacoustics are found in Schramm (2009) and Tosh *et al.* (2012).

The BEM has though a disadvantage, the increase of the number of elements with the second power of the frequency ($N \sim O(f^2)$) and the increase of storage capacity with $O(N^2)$ limits the range of application of the BEM to low and middle frequencies. Moreover, the fact that the system matrices are full populated and asymmetric inhibits the use of special techniques to invert matrices with special properties so that the number of arithmetic operations to solve the system using direct solvers increases with $O(N^3)$ ($O(N^2)$ with iterative solvers). In recent years, variants of the BEM have been proposed in order to extend the range of application of the method to higher frequencies. The variant which has drawn the major attention for its potential is the Fast Multipole BEM (FMBEM). The FMBEM applies iterative solvers to solve the system of equations and accelerates the matrix-vector multiplication to reduce the memory requirement to $O(N)$, the number of operations to $O(N \log^2 N)$ and the solution time to $O(N)$(see Liu, 2009). Other variants that have been proposed are the Wave BEM for scattering problems which includes the wave behaviour into the shape functions of the element and needs a much coarser mesh than the conventional BEM (Perrey-Debain *et al.*, 2003) or the Energy Boundary Element Analysis (EBEA) that can calculate the acoustic field generated at high frequency from a radiator with incoherent intensity boundary conditions (Wang *et al.*, 2004).

2. Basic concepts of the BEM

The BEM is based on the discretization of an integral equation derived from the original partial differential equation (deterministic, element-based method). The integral equation is defined on the boundary of the domain and relates the solution on the boundary to the solution at points in the domain. In acoustics, the differential equation is the wave equation in time domain or the Helmholtz equation in frequency domain.

We consider a three-dimensional body in free space with boundary Σ which is assumed to have a closed surface with an outward normal vector n. The exterior of Σ is denoted by V (see Fig. 1).

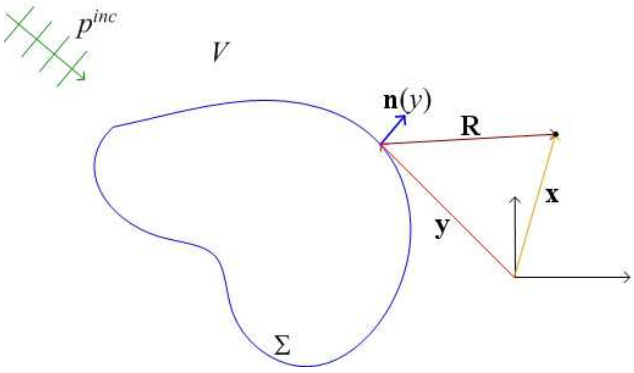

Fig. 1. Acoustic domain and boundary surface.

Equation (1) is the Helmholtz integral equation (HIE) and provides an expression for the sound pressure at every point x in V from the acoustic quantities at the surface Σ

$$c(\mathbf{x})p(\mathbf{x}) = p^{inc}(\mathbf{x}) + \int_{\Sigma} p(\mathbf{y}) \frac{\partial g(\mathbf{x},\mathbf{y})}{\partial n(\mathbf{y})} \,\mathrm{d}S(\mathbf{y}) - \int_{\Sigma} \frac{\partial p(\mathbf{y})}{\partial n(\mathbf{y})} g(\mathbf{x},\mathbf{y}) \,\mathrm{d}S(\mathbf{y}). \tag{1}$$

Here $g(\mathbf{x},\mathbf{y})$ is the free space Green's function

$$g(\mathbf{x},\mathbf{y}) = \frac{e^{-jkR}}{4\pi R}, \qquad R = |\mathbf{x}-\mathbf{y}|, \qquad j = \sqrt{-1} \tag{2}$$

with wavenumber k, $p^{inc}(\mathbf{x})$ is the incident pressure and $c(\mathbf{x})$ is the solid angle of the exterior volume at $\mathbf{x}$ given by

$$c(\mathbf{x}) = 1 + \frac{1}{4\pi} \int_{\Sigma} \frac{\partial}{\partial n(\mathbf{y})} \left(\frac{1}{R}\right) \mathrm{d}s(\mathbf{y}). \tag{3}$$

For points in the acoustic domain, $c(\mathbf{x})$ has the value 1. For points on the surface, if Σ is smooth, i.e. if there exists only one unique tangent plane at each point, the constant $c(\mathbf{x})$ has the value 0.5. For radiation problems, the incident sound pressure is zero.

If both p and $\partial p/\partial n$ are known on Σ, the sound pressure at points in V can be obtained simply by performing the integral (1). Usually, only one of the quantities is known and the other has to be calculated. Depending on which quantity is known, three types of boundary conditions (BCs) occur: a) Neumann BC: $\partial p/\partial n$ is given; b) Dirichlet BC: p is known, and c) Robin BC: a combination of p and $\partial p/\partial n$ is defined. In general, the whole surface consists of parts, on which different BCs are prescribed.

When the whole surface is equipped with a Dirichlet BC, Eq. (1) becomes a Fredholm integral equation of the first kind, which in its discretized form produces matrices that are often ill-conditioned. This case can be avoided if the normal derivative of Eq. (1)

$$\frac{1}{2}\frac{\partial p(\mathbf{x})}{\partial n(\mathbf{x})} = \frac{\partial p^{inc}(\mathbf{x})}{\partial n(\mathbf{x})} + \int\limits_{\Sigma} p(\mathbf{y})\frac{\partial^2 g(\mathbf{x},\mathbf{y})}{\partial n(\mathbf{x})\partial n(\mathbf{y})}\,\mathrm{d}S(\mathbf{y}) - \int\limits_{\Sigma} \frac{\partial p(\mathbf{y})}{\partial n(\mathbf{y})}\frac{\partial g(\mathbf{x},\mathbf{y})}{\partial n(\mathbf{x})\partial n(\mathbf{y})}\,\mathrm{d}S(\mathbf{y}) \qquad (4)$$

is considered, since this equation is a Fredholm integral equation of the second kind.

The kernels of Eqs. (1) and (4) possess singularities of different degrees. In Eq. (1), there is a weak singularity proportional to $1/R$ and a strong singularity proportional to $1/R^2$. Equation (4) has a strong singularity proportional to $1/R^3$. These three types of singularities need to be handled by using special techniques.

The numerical implementation of the BEM requires the discretization of the surface of the body and the corresponding integral equations. Therefore, Σ is divided in N nodes and Q elements. The acoustical quantities on the surface can be assumed to be constant inside each single element or be interpolated from the values at the nodes. The size of the resulting system of equations will be $N \times N$ in the node based case or $Q \times Q$ in the element based case.

In this paper, the second option, i.e. the use of constant elements is assumed. The integral equations are solved at the centroid of each element. We write Eqs. (1) and (4) for $c(\mathbf{x}) = 1/2$ in matrix form as

$$\left(\frac{1}{2}\mathbf{I} - \mathbf{D}\right) p + \mathbf{S}\frac{\partial p}{\partial n} = p^{inc}, \qquad (5)$$

$$\left(\frac{1}{2}\mathbf{I} + \mathbf{K}\right) \frac{\partial p}{\partial n} - \mathbf{M}p = \frac{\partial p^{inc}}{\partial n}, \qquad (6)$$

where I is the identity matrix and $\mathbf{S}$, $\mathbf{D}$, $\mathbf{K}$ and $\mathbf{M}$ are $Q \times Q$ matrices whose coefficients represent the interaction between two surface elements and are defined as:

$$S_{ij} = g_{ij}\,\mathrm{d}s_j, \qquad D_{ij} = \frac{\partial g_{ij}}{\partial n_j}\,\mathrm{d}s_j,$$

$$K_{ij} = \frac{\partial g_{ij}}{\partial n_i}\,\mathrm{d}s_j, \qquad M_{ij} = \frac{\partial^2 g_{ij}}{\partial n_i \partial n_j}\,\mathrm{d}s_j.$$

For obtaining accurate results, the discretized model should have at least six elements per wavelength λ. According to this rule of thumb, the number of elements Q increases proportionally to the square of the frequency (f^2) in three dimensions and the storage capacity required for the computations increases proportionally to f^4.

Since the BEM only requires the discretization of the surface of the body, it reduces the dimensions of the problem by one. This constitutes an advantage in comparison with the FEM which requires a discretization of the whole domain.

3. Exterior problems

The main advantage of the BEM over the FEM is the fact that the Green's function satisfies the radiation condition at infinity, i.e. the BEM can deal directly with unbounded domains. In contrast, the FEM requires special non-reflecting boundary conditions or regions with artificial high absorption (e.g. Perfectly Matched Layers). However, the BEM has also difficulties for exterior problems.

3.1. Non-uniqueness at certain frequencies

The solutions of the surface integral equations (SIEs) are not unique at a number of critical frequencies corresponding to internal resonances of the object. While the integral Eqs. (1) and (4) fail only at a discrete set of wavenumbers, the linear systems of Eqs. (5) and (6) become ill-conditioned when k is merely in the vicinity of a critical value. Under these conditions, severe loss of accuracy will be experienced. As the wavenumber k increases, so does the density of critical values, and hence it becomes increasingly difficult to get an accurate solution.

To overcome this problem, two approaches are usually employed, namely the CHIEF method (Schenk, 1968) and the Burton and Miller method (Burton, Miller, 1971).

In the CHIEF method, the integral equation (IE) is additionally formulated at a certain number of interior points, forcing the solution to fulfill the condition that the IE is zero in the interior. As a result, an over-determined system of equations has to be solved using, for example, the least squares technique. The advantage of this method is its simple implementation but its disadvantage is the need of a properly choice

of the position and number of "CHIEF-points". The interior points are not allowed to lie at nodal points and the number of points increases with the frequency due to the increase of the density of internal resonances.

In the Burton and Miller method, one uses a linear combination of the Eqs. (1) and (4). The coupling parameter γ has to have a non-zero imaginary part to ensure the uniqueness of the solution. Amini *et al.* (1992) found as a nearly optimal value $\gamma = j/k$. The system of equation to be solved is written as:

$$\left(\frac{1}{2}\mathbf{I} - \mathbf{D} - \gamma\mathbf{M}\right) p + \left(\mathbf{S} + \gamma\left(\frac{1}{2}\mathbf{I} + \mathbf{K}\right)\right) \frac{\partial p}{\partial n} = p^{inc} + \gamma \frac{\partial p^{inc}}{\partial n}. \tag{7}$$

Using this approach, the size of the system matrices is not enlarged. However, now it is needed to evaluate the hypersingular diagonal coefficients of $\mathbf{M}$.

The method of Dual Surface Integral Equations (DSIE) is an alternative method applied mostly in electromagnetics, but it can be also used to treat to acoustic problems as shown in Mohsen *et al.* (2011). The DSIE preserves the simplicity of CHIEF and specifies the location of the interior points to ensure uniqueness. It locates the interior points on a surface Σ_δ close to Σ constructed at a distance δ along the normal to the surface (see Fig. 2).

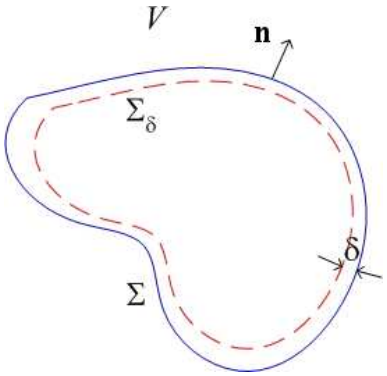

Fig. 2. Interior surface used in the DSIE method.

Similar to the Burton and Miller approach, the integral equation evaluated on the surface is combined with the one evaluated at the interior surface multiplied by a purely imaginary factor α to ensure the uniqueness. The DSIE in matrix form is given by

$$\left(\frac{1}{2}\mathbf{I} - \mathbf{D} - \alpha\overline{\mathbf{D}}\right) p + \left(\mathbf{S} + \alpha\overline{\mathbf{S}}\right) \frac{\partial p}{\partial n} = p^{inc} + \alpha\bar{p}^{inc}. \tag{8}$$

The matrices with an upper bar denote the matrices evaluated at the interior surface. The resulting system of equations does not contain the hypersingularities of Burton and Miller while preserving its square matrix form. A proof of uniqueness is given in Mohsen *et al.* (2011) which also states that δ should be less than $\lambda/2$.

We now present the application of the DSIE method to an acoustic radiation problem. Other examples can be found in Mohsen *et al.* (2011). The uniqueness of the solutions at all frequencies is ensured for a non-zero imaginary part of α and a maximum value of $\delta < \lambda/2$. However, optimal values are not known a priori for general configurations. In Mohsen *et al.* (2011), a parametric study of the values of α and δ was performed. The results showed that good accuracy was obtained in several cases using $\alpha = j$ and $\delta = \lambda/8$. In the following example, these values are chosen.

We consider a rectangular prism (cuboid) where one eighth of his volume is removed (see Fig. 3). The prism has a side $L = 1$ m and the analysis was made for frequencies that cover the range $kL = 9.1\ldots22$.

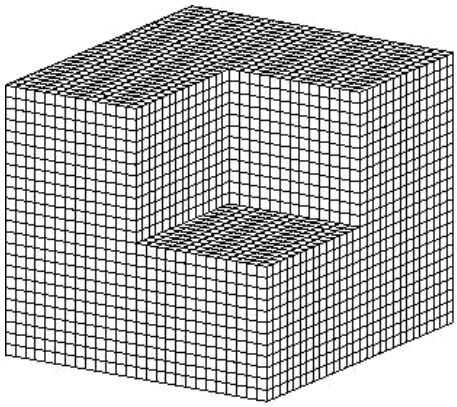

Fig. 3. Rectangular prism.

We assume that the normal velocity at the surface of the prism is due to a dipole located inside the body ($\mathbf{r}_d$). The sound pressure p_d and sound power W_d of the dipole are given by the expressions

$$p_d(\mathbf{r}) = h_1^{(2)}(k\,|\mathbf{r} - \mathbf{r}_d|) P_1^0(\cos\theta),$$
$$W_d = \frac{2\pi}{3\rho c k^2}, \tag{9}$$

where $h_1^{(2)}(\mathbf{x})$ is the spherical Hankel function of the second kind and first order, $P_1^0(x)$ is the associated Legendre function and θ is the angle between $(\mathbf{r} - \mathbf{r}_d)$ and the z-axis.

The radiated sound power level and the radiation pattern at $f = 779$ Hz are presented in Fig. 4. The DSIE method provides very good results. All irregular peaks of the sound power are eliminated and the typical eight-pattern of the dipole is very well reproduced at the critical frequency, whereas the normal Helmholtz integral equation gives completely wrong results.

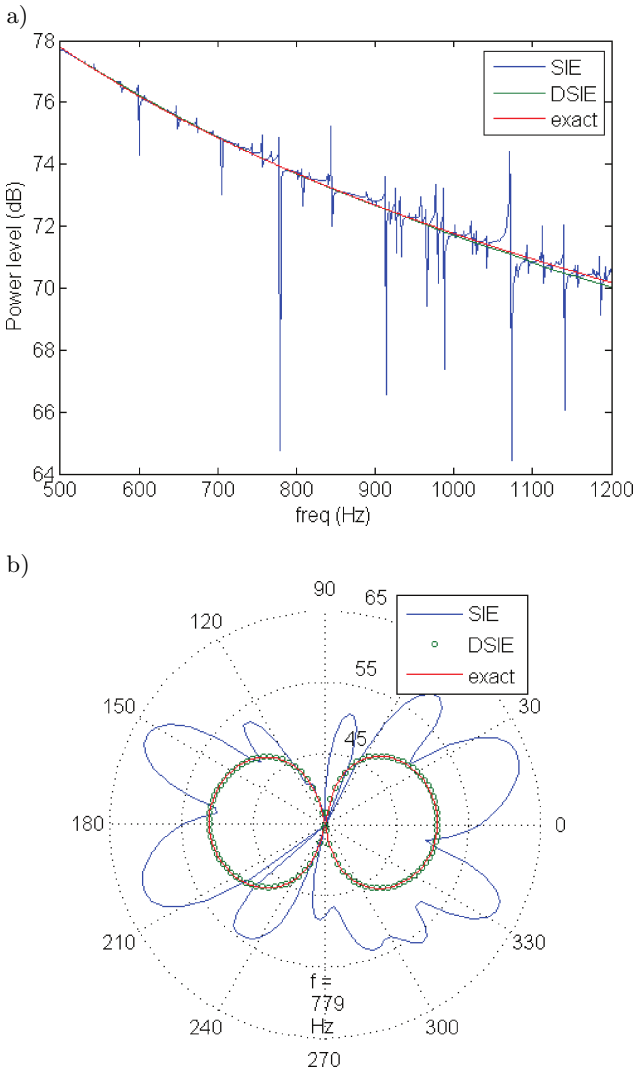

Fig. 4. Radiation of the rectangular body: a) sound power, b) directivity.

3.2. Half-space problems

Half-space problems are more realistic than free space problems. For those problems, in Eq. (1) or Eq. (4) the integration should include the object surface plus the surface of the infinite plane. The integration over the infinite plane can be avoided if a Green's function that satisfies the boundary condition on the plane is available. Hence, the integral equation for the half-space is written as

$$\begin{aligned} c(\mathbf{x})p(\mathbf{x}) = & \int_{\Sigma} p(\mathbf{y}) \frac{\partial g^h(\mathbf{x},\mathbf{y})}{\partial n(\mathbf{y})} \,\mathrm{d}S(\mathbf{y}) \\ & - \int_{\Sigma} \frac{\partial p(\mathbf{y})}{\partial n(\mathbf{y})} g^h(\mathbf{x},\mathbf{y}) \,\mathrm{d}S(\mathbf{y}) \\ & + p^{inc}(\mathbf{x}) + p^{ref}(\mathbf{x}), \end{aligned} \tag{10}$$

where $g^h(\mathbf{x},\mathbf{y})$ is the half-space Green's function and $p^{ref}(\mathbf{x})$ is the reflection of $p^{inc}(\mathbf{x})$ in absence of the body and $c(\mathbf{x})$ is given by Eq. (3) for all points except for those belonging simultaneously to Σ and to the infinite plane. For those particular points, the constant c is given by Seybert and Wu (1989)

$$c(\mathbf{x}) = 1 + \frac{1}{2\pi} \int_{\Sigma+\Sigma_c} \frac{\partial}{\partial n(\mathbf{y})} \left(\frac{1}{R}\right) \mathrm{d}s(\mathbf{y}). \tag{11}$$

Generally, the Green's function above an infinite plane with a surface impedance Z can be written as

$$g^h(\mathbf{x},\mathbf{y}) = \frac{e^{-jkR_1}}{4\pi R_1} + \frac{e^{-jkR_2}}{4\pi R_2} + C(\gamma) \tag{12}$$

with $\gamma = j\rho\omega/Z$, $R_1 = |\mathbf{x}-\mathbf{y}|$, $R_2 = |\mathbf{x}-\mathbf{y}^m|$, where $\mathbf{y}^m$ is the image source point with respect to the plane. Considering the infinite plane at the XY plane, if the source point is placed at $\mathbf{y} = (y_1, y_2, h)$, the image source point is placed at $\mathbf{y}^m = (y_1, y_2, -h)$. $C(\gamma)$ is a correction term due to the value of the impedance. The two limiting cases are a) rigid plane and b) soft plane. For the first one $C(\gamma) = 0$ and for the second one, the Green's function is written as

$$g^h(\mathbf{x},\mathbf{y}) = \frac{e^{-jkR_1}}{4\pi R_1} - \frac{e^{-jkR_2}}{4\pi R_2}. \tag{13}$$

In the literature, one can find different formulas for the correction term. One expression for $C(\gamma)$ has been derived in the work from Ochmann (2004):

$$C(\gamma) = \frac{j\gamma}{2\pi} \int_{-\infty}^{0} \left(\frac{e^{-jk\sqrt{x^2+y^2+(z+h+j\zeta)^2}}}{\sqrt{x^2+y^2+(z+h+j\zeta)^2}} \right) e^{j\gamma\zeta} \,\mathrm{d}\zeta. \tag{14}$$

The line integral can be interpreted as the superposition of source functions along an "imaginary z-axis" at the points $z = -h - j\zeta$. The main advantage of this formula is that the line integral is convergent for all kind of surface impedances on the infinite plane. For points very near to the plane and for low frequencies, the integrand oscillates strongly and the computation can be time consuming. It is also possible to find exact solutions for the Green's function for moving monopole above impedance planes (Ochmann, 2013) or for a steady point source in time domain (Ochmann, 2011). An overview about such halfspace-Green's functions can be found in (Ochmann, 2013).

An example of the application of the half-space BEM is the computation of the so-called horn effect. The horn effect is an amplification of the sound radiation of the source due to the hornlike geometry of a tyre/road interface. In the numerical implementation of the method, the integration over the elements lying very near the plane requires especial attention (e.g. adapted integration, finer re-meshing, etc.). A comparison between numerical simulations and measurements (see Fig. 5) shows good agreement for two types of

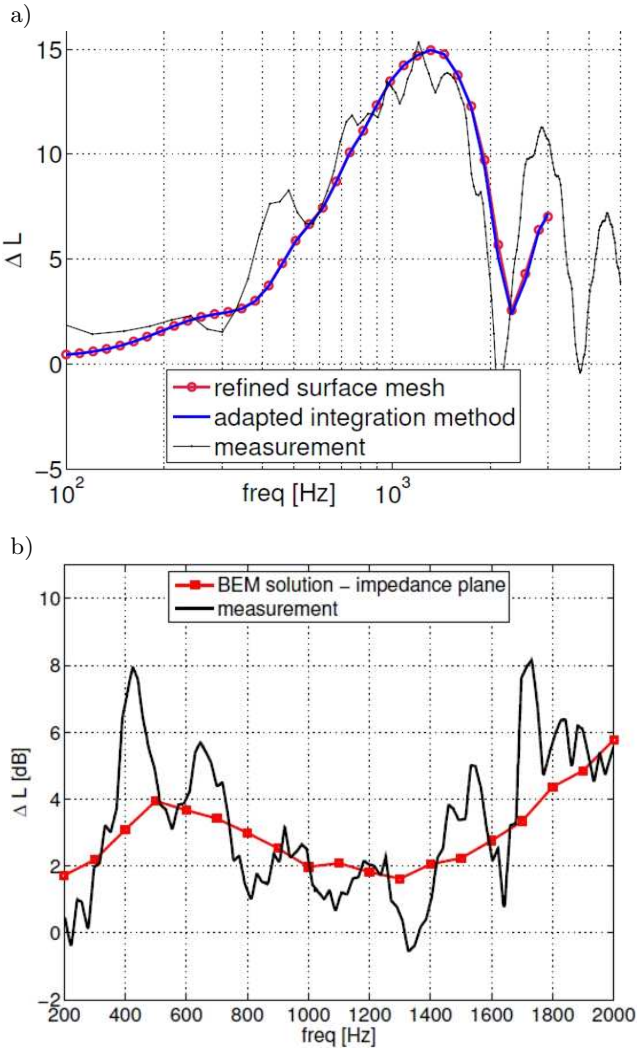

Fig. 5. Amplification due to the horn effect: a) for a rigid surface, b) for an absorbing surface (taken from (Brick, 2011)).

planes, rigid and absorbing (Brick, 2011). The larger deviations in the second case may be due to the reverberant environment and the finite size of the real absorbing layer (mineral wool).

The sound level difference ΔL is defined as

$$\Delta L = 20 \log \left| \frac{p_{\text{with tyre}}}{p_{\text{no tyre}}} \right|. \tag{15}$$

4. Interior problems

The computation of the sound field in bounded domains does not have any feature different to the exterior problem. The resonances in this case are real. If no absorption at the boundaries is considered, the results will not be accurate around the resonances, but if there is enough absorption, no additional care should be taken.

An example of the application of the BEM for interior problems is the study of the sound field in a homogenizer. An ultrasonic homogenizer consists on an electronic generator, a transducer and a horn. When the horn is introduced in a fluid, the longitudinal oscillations of the horn tip produce sound waves that propagate through the medium. The intense sound pressure produces phenomena like streaming, cavitation, turbulence and shock waves. All these different mechanisms contribute to reduce small particles in the liquid improving uniformity and stability. A simulation of all physical processes mentioned before would be a very difficult task. However, knowledge of the sound field distribution is useful, since regions of higher pressure are related to regions of high cavitation.

The sound pressure distribution in a glass vessel with a special geometry was studied. The vessel has a conical shape with three narrow hollow handles connecting the upper and lower parts of the vessel. Figure 6 shows one third of the model.

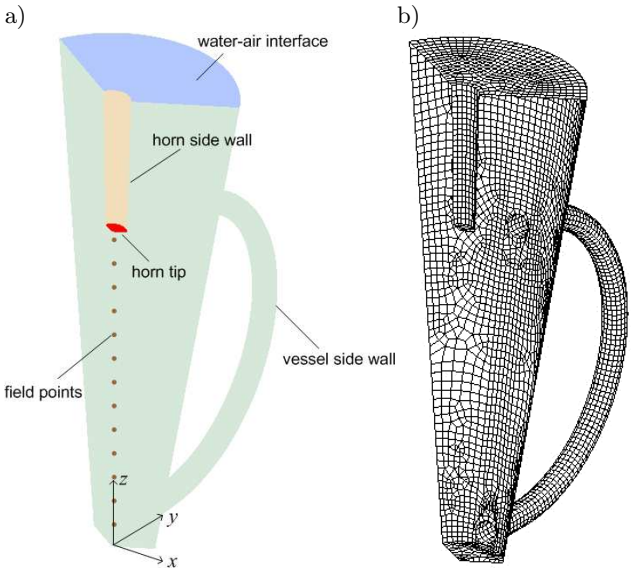

Fig. 6. One-third model of ultrasonic homogenizer: a) boundary conditions in the acoustic model, b) mesh used for the numerical calculations.

The ultrasonic horn vibrates at 20 kHz. The vessel is partially filled with water. Since the sound speed in water is 1500 m/s, the wavelength is about 7.5 cm. We thank the Bandelin electronic GmbH & Co. KG, which provided us with the model of the vessel and the sonotrode.

The glass walls of the vessel can be considered as soft if they are thin or as rigid if they are thick (Yasui *et al.*, 2007). The interface liquid-air can be also considered as soft (Klima *et al.*, 2007).

Two aspects were studied: the effect of the boundary condition at the wall of the vessel and the influence of the handles on the pressure distribution.

The sound pressure was calculated at several field points in the middle of the vessel just below the horn tip.

Figure 7 shows the sound pressure at the field points. The plot in 7a shows the effect of the boundary condition. The pressure was computed considering in one case rigid walls, and in a second case soft walls. The pressure distributions differ significantly, meaning that a proper determination of the boundary condition is required. A more accurate result can be obtained if a coupling between fluid and structure is considered. No absorption in the fluid was considered. The plot 7b shows that the presence of the handles has a minor influence on the sound pressure in the vessel when hard walls are considered. There is no influence at all when soft walls are assumed. The presence of the handles has an influence on the fluid circulation. Figure 8 shows the pressure distributions on the surface elements computed by the BEM.

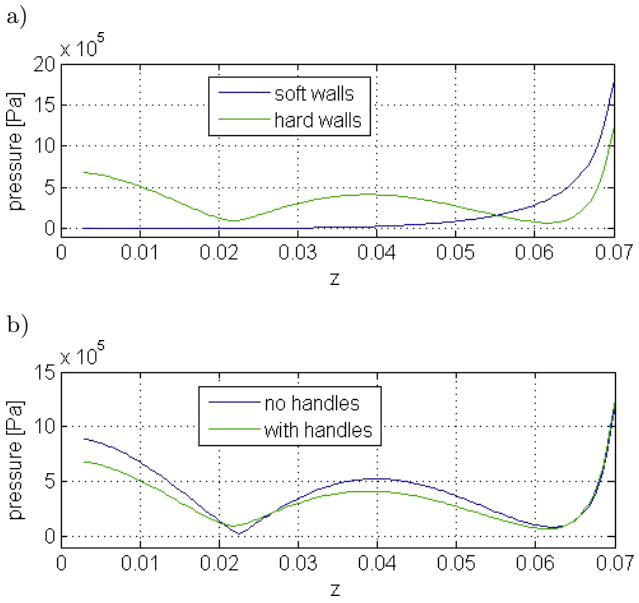

Fig. 7. Sound pressure at the field points: a) comparison between different boundary conditions at the walls, b) comparison between vessel without handles and with handles.

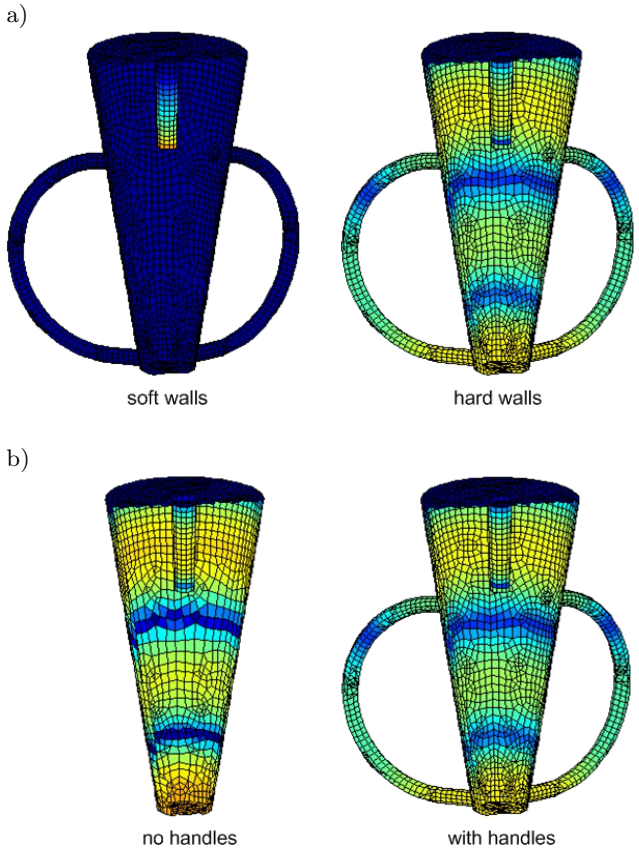

Fig. 8. Sound pressure level on the surface: a) comparison between different boundary conditions at the walls, b) comparison between vessel without handles and with handles.

5. Acoustic-structure interaction

The BEM can be coupled to the Finite Element Method (FEM) to handle problems involving acoustic-structure interaction. As an example of such coupling, we consider the computation of the transmission loss (TL) of thin structures.

When thin structures are studied, it is more convenient to use 2D shell elements in a FEM calculation instead of 3D solid elements. If sound radiation from both sides of a thin structure is considered, a so-called indirect BEM approach has to be applied.

5.1. Thin plate in a duct

In a first numerical experiment, the thin plate is placed in a duct. The acoustic domain is divided in two subdomains: behind and in front of the plate. Two integral equations are solved, one in each subdomain. The equations are coupled through the motion of the plate.

Figure 9 shows the two computational domains Ω_I and Ω_{II} and the five different surfaces of the model with their respective normal vectors. The boundary conditions on all surfaces are listed in Table 1.

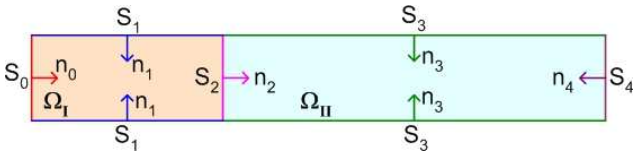

Fig. 9. Sound field in Kundt's tube.

Table 1. Boundary conditions.

Surface	Description	Boundary condition
S_0	loudspeaker	$v_n = v_L$
S_1, S_3	side wall	$v_n = 0$
S_2	plate	$\partial p_I/\partial n = \partial p_{II}/\partial n = \rho\omega^2 u_P$
S_4	termination	$Z = Z_t$

The boundary integral equations in Ω_I and Ω_{II} are given by

$$C_I p_I = \int_{S_0} \left(p_{I0} \frac{\partial g}{\partial n} + j\rho\omega v_L g \right) \mathrm{d}S + \int_{S_1} p_{I1} \frac{\partial g}{\partial n} \mathrm{d}S - \int_{S_2} \left(p_{I2} \frac{\partial g}{\partial n} - \rho\omega^2 u_P g \right) \mathrm{d}S, \tag{16}$$

$$C_{II} p_{II} = \int_{S_2} \left(p_{II2} \frac{\partial g}{\partial n} - \rho\omega^2 u_P g \right) \mathrm{d}S + \int_{S_3} p_{II3} \frac{\partial g}{\partial n} \mathrm{d}S + \int_{S_4} p_{II4} \left(\frac{\partial g}{\partial n} - \frac{j\rho\omega g}{Z_t} \right) \mathrm{d}S \tag{17}$$

and the equation of motion of the plate

$$(K - \omega^2 M) u_P = F. \tag{18}$$

p_{I0}, p_{I1}, p_{II3} and p_{II4} are the pressures on the walls, p_{I2} and p_{II2} are the pressures at both sides of the plate and u_P is the normal displacement of the plate.

Discretizing Eqs. (16) and (17) on all surfaces and combining the system of equations with Eq. (18), the sound pressure and the normal velocity of the plate can be computed.

The transmission loss (TL) of the plate is defined as

$$TL = -10 \lg(\tau), \qquad \tau = \frac{W_t}{W_i}, \tag{19}$$

where τ is the transmission coefficient and W_t and W_i are the transmitted and incident sound power, respectively.

The TL obtained from measurements is determined assuming only plane wave propagation, therefore, this method is valid only below the first cut-on frequency. The TL is computed from the pressure values obtained by three microphones assuming an anechoic termination. In the simulation, the TL is obtained emulating the measurement procedure. By the numerical simulations, an anechoic termination can be easily implemented while in real measurements an anechoic termination may be difficult to accomplish.

In the downstream section of the duct, only a plane wave in the $+x$ direction propagates while in the upstream section two plane waves propagate in the $+x$ and $-x$ directions respectively (see Fig. 10).

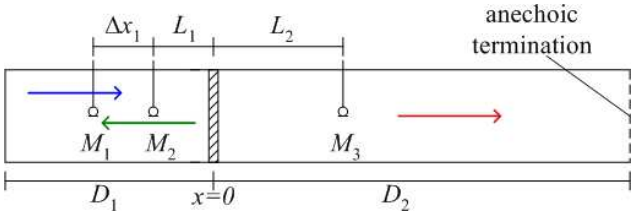

Fig. 10. Plane waves and microphone positions.

The transmission coefficient τ can be expressed in terms of the sound pressure at the microphones p_{M1}, p_{M2} and p_{M3} as:

$$\tau = \frac{|2 \sin k\Delta x_1|^2 \, |p_{M_3}|^2}{|p_{M_1} - p_{M_2} e^{-jk\Delta x_1}|^2}. \tag{20}$$

The results of (20) will be accurate under the condition that $\Delta x_1 < c/f$.

The transmission loss of a 1 mm thick aluminium plate was simulated. The plate was placed in a 4 m long duct with square cross section (0.25 m side length). The anechoic termination was implemented by using the free field impedance $Z = \rho c$ on S_4. The sound pressure in the duct was determined using (16) and (17) and the transmission coefficient was computed using (20). To validate the numerical model, the results of the simulation were compared with the results of a measurement. Since the plate was fixed to the duct walls using an adhesive material, an "elastic BC" was assumed. The rigidities of the translational and rotational springs were chosen in such a way that a good agreement between simulation and measurement is obtained. Fig. 11 shows the comparison of simulated and measured TL.

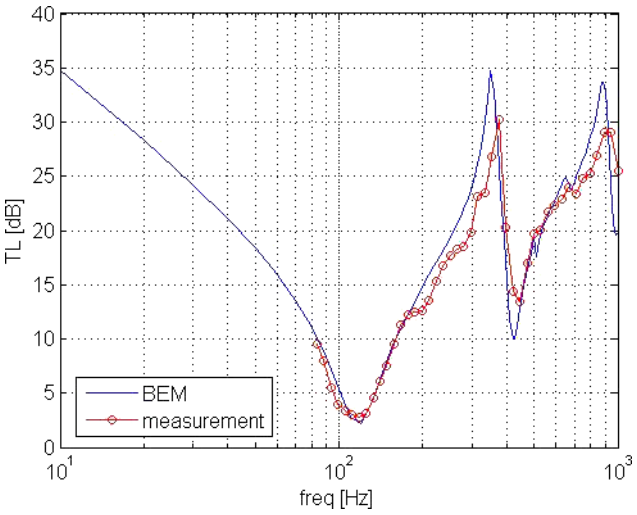

Fig. 11. Comparison of simulation and measurement.

5.2. Plate in a test facility

In a second numerical experiment, the thin plate is placed in a test facility. The test facility consists in a source room and a receiver room connected by an opening where the specimen is placed. Equation (19) cannot be used to determine the TL, since incident and transmitted power cannot be determined due to the reflections from the walls. For specimens measured in test facilities, the TL is determined through pressure or intensity measurements. Three formulas found in the norms were tested and the corresponding results were compared.

5.2.1. TL from pressure levels

The norm DIN EN ISO 10140-2 defines the transmission loss by the expression

$$R_p = L_1 - L_2 + 10\lg\left(\frac{S}{A}\right), \tag{21}$$

where L_1 is the mean pressure level in source room in dB, L_2 the mean pressure level in receiving room in dB, S the area of the opening where the element is mounted (in m^2) and A the equivalent absorbing area in the receiving room (in m^2).

Equation (21) requires that the sound fields in both rooms are diffuse and that the sound in the receiving room is exclusively due to the sound coming through the test element.

According to the norm DIN EN ISO 10140-4, the spatial averaged sound pressure level is defined as

$$L = 10\lg\left(\frac{1}{n}\sum_{i=1}^{n}\frac{p_i^2}{p_0^2}\right), \tag{22}$$

where n is the number of microphone positions in the room, p_i the rms value of the pressure and $p_0$is a reference pressure (in air $p_0 = 2\cdot 10^{-5}$ Pa). The norm recommends placing the microphones outside the direct field (e.g. a minimum of 1 m from the source) and at least 0.7 m away from the room borders and 1 m away from the specimen. The separation between microphone positions should be greater than 0.7 m. A minimum of 5 positions distributed in the room has to be considered, but they should not form a regular grid and no pair of microphones should lie in the same plane parallel to the room borders.

A diffuse sound field is to be produced by loudspeakers in at least two positions or by a single loudspeaker moved to at least two positions. At low frequencies, especially below 100 Hz, the minimum number of loudspeakers increases to three. The sound field should be constant and have a uniform spectrum, i.e. the difference in the pressure level between adjacent 1/3-octave bands should not exceed 6 dB. The lack of diffusivity can be compensated by averaging the sound pressure obtained by different source positions. The norm recommends positions at least 0.7 m away from the room borders. The separation between source positions should be greater than 0.7 m, no pair of sources should lie in the same plane parallel to the room borders or be symmetric respect to the middle planes.

5.2.2. TL from pressure and intensity levels

The norm DIN EN ISO 15186-1 defines an expression that includes the case that the receiving room can be replaced by the open space. For this reason, the method considers the sound intensity measured on a surface involving completely the specimen at the receiving side S_m. The formula reads

$$R_I = L_1 - 6 - \left[L_I + 10\lg\left(\frac{S_m}{S}\right)\right], \tag{23}$$

where L_I is the normal intensity level averaged over S_m.

Equation (23) requires that the normal distance d, between partition and enveloping surface lies in the range $0.1 < d < 0.3$ and the difference between the intensity level and pressure level satisfies $0 < L_p - L_I < 10$ dB.

5.2.3. TL at low frequencies

In rooms with small volumes and not favourable dimensions is not always possible to obtain reliable results at low frequencies using (21) or (23). Both require that at least one room dimension contains a wavelength and another room dimension at least a half wavelength of the lowest band middle frequency.

For frequencies between 50 and 160 Hz, the norm DIN EN ISO 15186-3 introduces the following formula for R

$$R_{low} = L_{pS} - 9 - \left[L_I + 10\lg\left(\frac{S_m}{S}\right)\right], \tag{24}$$

where L_{pS} is the mean pressure level in the source room averaged over the surface of the partition.

5.2.4. Comparison of R_p, R_I and R_{low}

To compare the results from (21), (23) and (24), 10 source positions, 30 microphone positions in the source room and 24 microphone positions in the receiving room meeting the norm recommendations were considered.

In Fig. 12, all source and microphone positions, the partition and the enveloping surface used for the intensity measurements are shown.

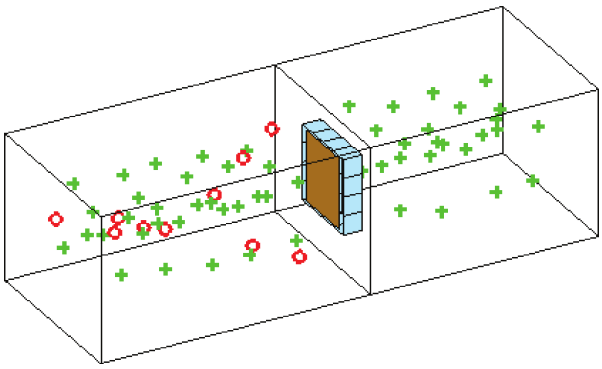

Fig. 12. Source positons (o) and microphone positions (+).

According to the norm 10140-4, one calculation is performed for each source position and the averaged transmission loss $\langle R\rangle$ is determined using the formula

$$\langle R\rangle = -10\lg\left(\frac{1}{Q}\sum_{i=1}^{Q}10^{-R_i/10}\right), \tag{25}$$

where Q is the number of source points.

The curves of transmission loss R_i and the averaged value $\langle R\rangle$ were calculated for 1/3-octave bands

from 31.5 Hz up to 800 Hz. The 1/3-octave band sound levels are obtained from the narrow band values using the expression

$$L_{1/3} = \left(\frac{1}{n_{1/3}} \sum_{i=1}^{n_{1/3}} \frac{p_i^2}{p_0^2} \right), \tag{26}$$

where $n_{1/3}$ is the number of frequencies in the 1/3-octave band. In this calculation, $n_{1/3} = 8$ for all bands.

The first 3 plots in Fig. 13 show the curves of R for each source position (coloured solid lines) and the mean value (dotted black line). The last plot shows a comparison between the mean values. These results show the sensitivity of expressions (21) and (23) to the source position at low frequencies and confirm their validity above 100 Hz. The expression (24) is completely independent of the source position not only below 100 Hz but at all frequencies. The mean values of R obtained by the three expressions are very similar.

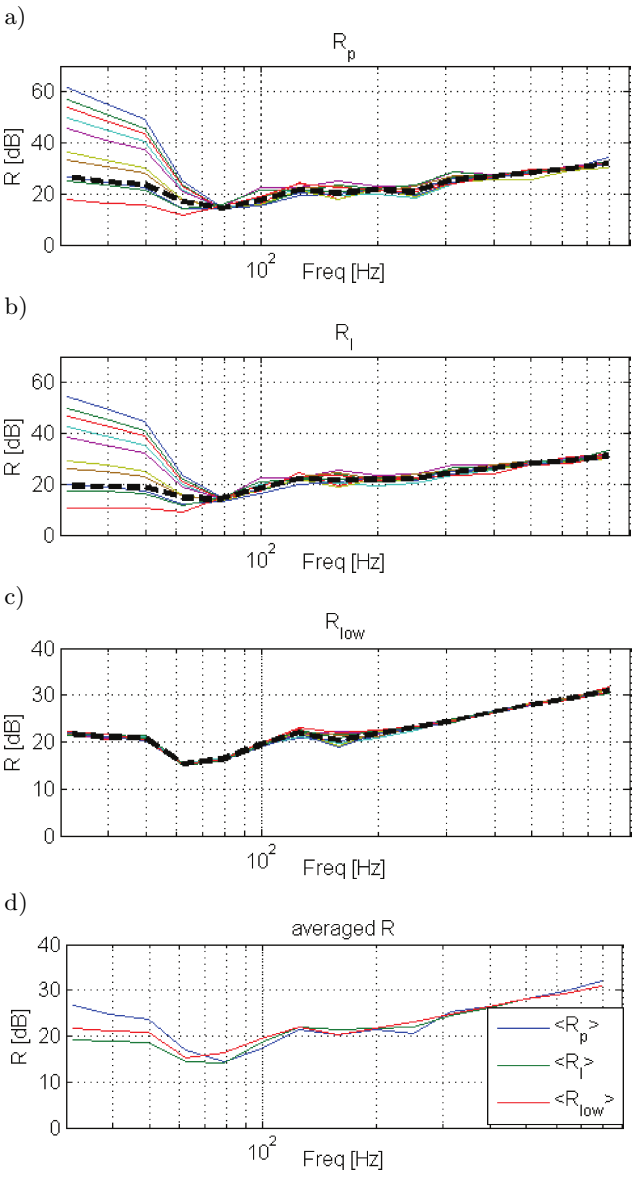

Fig. 13. Transmission loss curves obtained with different source positions using: a) Eq. (21), b) Eq. (23), c) Eq. (24). The averaged values of all source positions are shown in d).

Looking at the sound pressure distribution in the source room (Fig. 14), we find that at low frequencies the microphones are placed always in the direct field of the source. Therefore, it is expected that the results differ significantly from one position of the source to another.

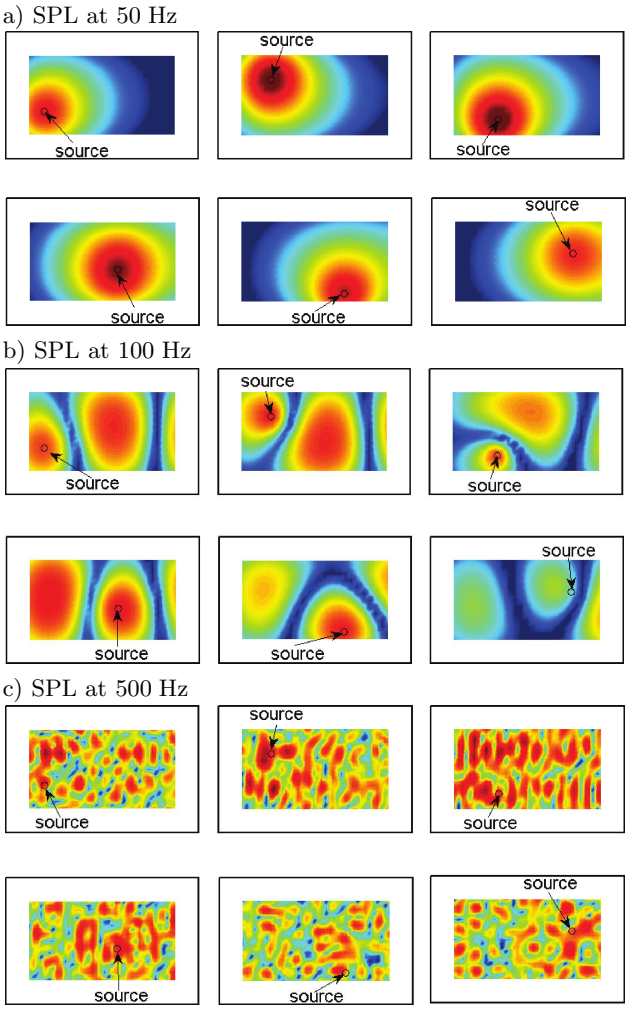

Fig. 14. Pressure level distributions in the source room at three frequencies for six different source positions.

6. Flow acoustics

Industrial and general engineering applications often include the presence of flows. Flows can affect the sound propagation but can also generate sound themselves.

6.1. Compact sources

Usual BEM implementations assume a medium at rest and simple sound sources like point sources or plane waves. The usual methods can be directly applied to problems containing flow if the region of sound

sources is spatially limited, so that a fictitious surface can be considered which encloses all sources and inhomogeneities. In the work from Piscoya *et al.* (2008), the sound radiation from an open jet flame was computed. A cylindrical surface enclosed the flame, and the boundary condition was the normal velocity of the fluid obtained by a Large-Eddy-Simulation (LES).

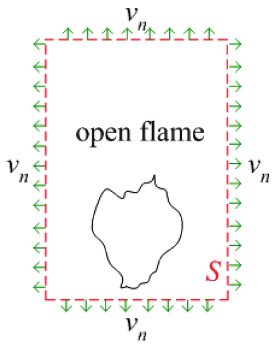

Fig. 15. Flame enclosed by a control surface.

Since the LES data were given in time domain, they had to be previously Fourier transformed into the frequency domain. In order to compare the simulated results with measurements, the complete simulated time series was divided into sub-series. A BEM calculation was performed with each sub-series and thereafter averaged to obtain the final result. Fig. 16 shows a comparison of the simulated and measured sound power. A reasonable agreement was obtained.

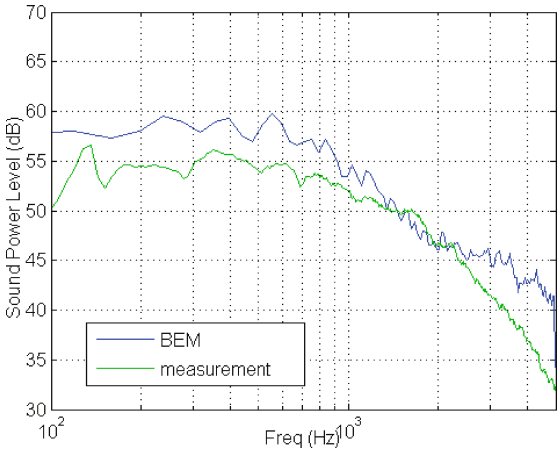

Fig. 16. Simulated and measured sound power of the flame.

To achieve good accuracy it was seen that it is very important to provide the correct acoustic boundary condition. Therefore, a separation of acoustic and hydrodynamic components in the flow (splitting technique) should be previously performed (Piscoya, Ochmann, 2009).

6.2. Uniform mean flow

Special implementations of the BEM can solve problems including the flow under the condition that the sound propagation does not affect the flow (weak coupling or one-way coupling).

If the flow (or in many cases the mean flow) can be assumed to be constant, a convective Helmholtz equation describes the sound propagation

$$\nabla^2\phi - 2jk(\mathbf{M}_a\cdot\nabla)\phi - (\mathbf{M}_a\cdot\nabla)^2\phi + k^2\phi = 0, \quad (27)$$

where ϕ is the velocity potential and $\mathbf{M}_a$ is the Mach number $\mathbf{M}_a = \mathbf{v}/c$.

Introducing the Green's function of the form

$$g(\mathbf{x},\mathbf{y}) = \frac{e^{-jk(R-\beta)/(1-M^2)}}{4\pi R}, \quad (28)$$

where

$$\beta = \mathbf{M}_0\cdot(\mathbf{x}-\mathbf{y}), \qquad R = \sqrt{(1-M^2)\,|\mathbf{x}-\mathbf{y}|^2 + \beta^2},$$
$$M^2 = |\mathbf{M}_a|^2$$

the integral form of Eq. (27) is given by

$$c(\mathbf{x})\phi(\mathbf{x}) = \int_\Sigma \Bigg[\Bigg(\frac{\partial g(\mathbf{x},\mathbf{y})}{\partial n(\mathbf{y})} + 2jk(\mathbf{M}_a\cdot\mathbf{n}(\mathbf{y}))g(\mathbf{x},\mathbf{y}) - (\mathbf{M}_a\cdot\mathbf{n}(\mathbf{y}))(\mathbf{M}_a\cdot\nabla_y g(\mathbf{x},\mathbf{y}))\Bigg)\phi(\mathbf{y}) - \frac{\partial\phi(\mathbf{y})}{\partial n(\mathbf{y})}\left(1-(\mathbf{M}_a\cdot\mathbf{n}(\mathbf{y}))^2\right) g(\mathbf{x},\mathbf{y})\Bigg]\,\mathrm{d}s(\mathbf{y}) \quad (29)$$

with

$$\mathrm{c}(\mathbf{x}) = 1 - \int_\Sigma \left[(\mathbf{M}_a\cdot\mathbf{n}(\mathbf{y}))\,(\mathbf{M}_a\cdot\nabla_y \mathrm{G}(\mathbf{x},\mathbf{y})) - \frac{\partial \mathrm{G}(\mathbf{x},\mathbf{y})}{\partial \mathrm{n}(\mathbf{y})}\right]\mathrm{d}s(\mathbf{y})$$

and $G = \dfrac{1}{4\pi R}$.

Equation (29) is then solved in the same way as the usual BEM. Figure 17 shows the sound pressure of a dipole. The model was a sphere where its normal surface velocity equals the velocity of a dipole.

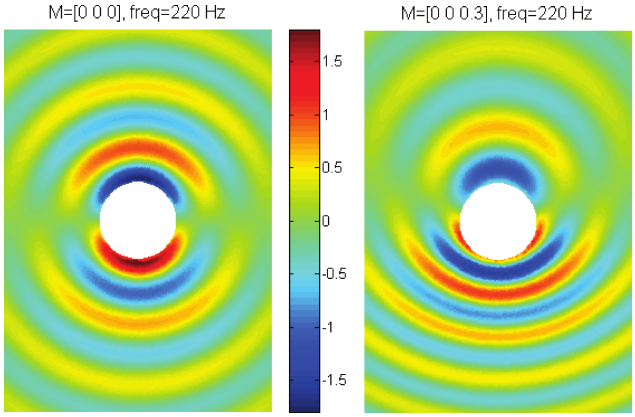

Fig. 17. Sound pressure due to a dipole; left: medium at rest; right: in a flow $M = 0.3$.

6.3. Non-uniform mean flow

A more general but also more complex problem arises when the flow in certain region of the domain (usually near the sound sources) is not uniform. In that case, the convected Helmholtz equation is not valid anymore and another equation including usually non-linear terms is required. For this type of problems, a special implementation of the BEM called the Dual Reciprocity BEM (DRBEM) can be used, but knowledge of the flow from physical considerations or from previous flow simulations (CFD), is needed. First, the governing equation has to be rewritten in a way that the left hand side has the same form as (27) and all other remaining terms are moved to the right hand side. Proceeding in such a way, an inhomogeneous convective equation with a source term b, which may also depend on the unknown velocity potential ϕ, is obtained. The integral form of this new equation will be equal to (29) plus an additional term given by a volume integral

$$-\int_{\Omega} b(\phi, \mathbf{M}_a) g(\mathbf{x}, \mathbf{y})\, \mathrm{d}V(\mathbf{y}). \tag{30}$$

In order to solve Eq. (30), $\mathbf{M}_a$ has to be known, as previously mentioned.

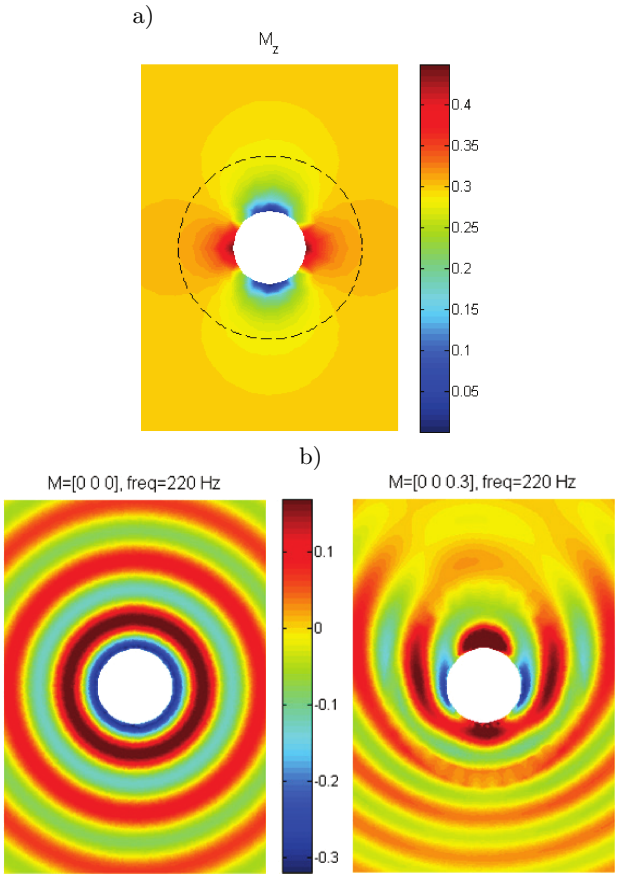

Fig. 18. a) z-component of the Mach number; b) pulsating sphere in medium without flow (left) and with non-uniform flow (right).

In the second step, the DRBEM is introduced. By expanding the source term b in known functions f_μ associated to the functions ψ_μ that satisfy the equation:

$$\nabla^2\psi_\mu - 2jk(\mathbf{M}_\infty \cdot \nabla)\psi_\mu - (\mathbf{M}_\infty \cdot \nabla)^2\psi + k^2\psi_\mu = f_\mu, \tag{31}$$

where $\mathbf{M}_\infty = \langle \mathbf{M}_a \rangle$, and applying the Green's identity, the volume integral can be replaced by a series of surface integrals. The final integral equation contains only surface integrals which are solved using the usual BEM procedure. Details of the method can be found in Lee *et al.* (1994). Figure 18 shows the distribution of the component M_z of the flow and the sound pressure of a pulsating sphere without and with flow.

7. Conclusions

The BEM is a powerful tool for acoustical simulations. The method is especially useful to solve free-space and half-space problems since no additionally non-reflecting boundary conditions are needed. It faces some difficulties like the appearance of critical frequencies or singularities, but they can be overcome by applying special techniques. Coupling to other methods like FEM for acoustic-structure interaction and CFD for aero-acoustic radiation is feasible. The method is limited today to low and middle frequencies due to the size of the models and the nature of the matrices involved (full-populated, complex, unsymmetric). Incorporating special tailored Green's functions can lead to very efficient variants of the BEM, e.g. for sound propagation above in half-spaces above impedance planes

Acknowledgments

The authors would like to thank Mrs. Aoki from the Institut für Bauphysik in Stuttgart for providing the data of the measured transmission loss.

This work has been partially supported by the German Research Foundation (DFG) within the project "Comprehensive computational model for sound transmission problems", and by the Berliner Senate Department for Economy, Technology and Research and the European Social Fund.

References

1. Amini S., Harris P., Wilton D. (1992), *Coupled Boundary and Finite Element Methods for the Solution of the Dynamic Fluid-Structure Interaction Problem*, Springer-Verlag, 40–56.
2. Baulac M., Defrance J., Jean P., Minard F. (2006), *Efficiency of Noise Protections in Urban Areas: Predictions and Scale Model Measurements*, Acta Acustica United with Acustica 92, 530–539.
3. Bolejko R., Dobrucki A. (2006), *FEM and BEM computing costs for acoustical problems*, Archives of Acoustics, **31**, 2, 193–212.

4. Brick H. (2009), *Application of the Boundary Element Method to combustion noise and half-space problems*, Ph.D Thesis, Chalmers University of Technology, Göteborg, Sweden.
5. Burton A.J., Miller G.F. (1971), *The application of integral equation methods to numerical solution of some exterior boundary-value problems*, Proc. R. Soc. Lond. A, **323**, 201–210.
6. Dobrucki A.B., Plaskota P. (2007), *Computational modelling of head-related transfer function*, Archive of Acoustics, **32**, 659–682.
7. Klima J., Frias-Ferrer A., Gonzalez-Garcia J., Ludvik J., Saez V., Iniesta J. (2007), *Optimisation of 20 kHz sonoreactor geometry on the basis of numerical simulation of local ultrasonic intensity and qualitative comparison with experimental results*, Ultrason. Sonochem., **14**, 19–28.
8. Lee L., Wu T.W., Zhang P. (1994), *A dual-reciprocity method for acoustic radiation in a subsonic non-uniform flow*, Engineering Analysis with Boundary Elements, **13**, 365–370.
9. Liu Y. (2009), *Fast Multipole Boundary Element Method: Theory and Applications in Engineering*, Cambridge University Press.
10. Mohsen A., Piscoya R., Ochmann M. (2011), *The application of the dual surface method to treat the non-uniqueness in solving acoustic exterior problems*, Acta Acustica United with Acustica, **97**, 4, 699–707.
11. Monazzam M.R., Naderzadeh M., Nassiri P., Fard S.M.B. (2010), *Performance of Environmental T-shape Noise Barriers Covered with Primitive Root Diffusers*, Archives of Acoustics, **35**, 4, 565–578.
12. Ochmann M. (2004), *The complex equivalent source method for sound propagation over an impedance plane*, J. Acoust. Soc. Am., **116**, 6, 3304–3311.
13. Ochmann M. (2011a), *Closed form solutions for the acoustical impulse response over a masslike or an absorbing plane*, J. Acoust. Soc. Am., **129**, 6, 3502–3512.
14. Ochmann M. (2011b), *Transient Green's functions above infinite impedance planes*, Proceedings Forum Acusticum 2011, Aalborg, Denmark, 241–246.
15. Ochmann M. (2013a), *Exact solutions for sound radiation from a moving monopole above an impedance plane*, J. Acoust. Soc. Am., **133**, 4, 1911–1921.
16. Ochmann M. (2013b), *Modelling of acoustical Green's functions above impedance planes by a superposition integral*, Proceedings AIA-DAGA 2013, Meran.
17. Piscoya R., Brick H., Ochmann M., Költzsch P. (2008), *Equivalent Source Method and Boundary Element Method for Calculating Combustion Noise*, Acta Acustica United with Acustica, **94**, 514–527.
18. Perrey-Debain E., Trevelyan J., Bettes P. (2003), *Plane wave interpolation in direct collocation boundary element method for radiation and wave scattering: numerical aspects and applications*, Journal of Sound and Vibration, **261**, 839–858.
19. Piscoya R., Ochmann M. (2009), *Separation of acoustic and hydrodynamic components of the velocity for a CFD-BEM hybrid method*, Proceedings of the NAG/DAGA 2009, Rotterdam, Netherlands.
20. Rausch M., Kaltenbacher M., Landes H., Lerch R. (2002), *Combination of finite and boundary element methods in investigation and prediction of load-controlled noise of power transformers*, Journal of Sound and Vibration, **250**, 323–338.
21. Schenk H.A. (1968), *Improved integral equation formulation for acoustic radiation problems*, J. Acoust. Soc. Am., **44**, 41–58.
22. Schramm C. (2009), *A boundary element extension of Curle's analogy for non-compact geometries at low-Mach numbers*, Journal of Sound and Vibration, **322**, 264–281.
23. Seybert A.F., Wu T.W. (1989), *Modified Helmholtz integral equation for bodies sitting on an infinite plane*, J. Acoust. Soc. Am., **85**, 1, 19–23.
24. Seybert A.F., Wu T.W., Li W.L. (1990), *Structural Acoustics Applications of the BEM and the FEM*, Boundary Element Methods in Engineering, Springer-Verlag, 536–542.
25. Suzuki S., Maruyama S., Ido H. (1989), *Boundary element analysis of cavity noise problems with complicated boundary conditions*, Journal of Sound and Vibration, **130**, 79–96.
26. Tadeu A., Simões I., António J., Sousa L. (2012), *Simulation of the 3D Sound Pressure Level Inside Closed Absorbing Acoustic Rooms Bounded by Non-Parallel Floor and Ceiling Surfaces, and Parallel Side walls*, Acta Acustica United with Acustica, **98**, 894–906.
27. Tinnsten M., Jonsson M., Johansson Ö. (2001), *Prediction and Verification of Acoustic Radiation*, Acta Acustica United with Acustica, **87**, 117–127.
28. Tosh A., Liever P., Owens F, Liu Y. (2012), *A High-Fidelity CFD/BEM Methodology for Launch Pad Acoustic Environment Prediction*, AIAA Paper, 2012–2107.
29. Utsuno H., Wu T.W., Seybert A.F., Tanaka T. (1990), *Prediction of sound fields in cavities with sound absorbing materials*, AIAA Journal, **28**, 1870–1876.
30. Wang A., Vlahopoulos N., Wu K. (2004), *Development of an energy boundary element formulation for computing high-frequency sound radiation from incoherent intensity boundary conditions*, Journal of Sound and Vibration, **278**, 413–436.
31. Wu T.W. (2000), *Boundary Element Acoustics: Fundamentals and Computer Codes*, WIT Press, Chapter 6.
32. Yasui K., Kozuka T., Tuziuti T., Towata A., Iida Y. (2007), *FEM calculation of an acoustic field in a sonochemical reactor*, Ultrason. Sonochem., **14**, 605–614.